Journal of
Applied Crystallography

ISSN 0021-8898

Received 27 July 2010
Accepted 4 November 2010

Supercritical carbon dioxide behavior in porous silica aerogel

Salvino Ciccariello,[a]* Yuri B. Melnichenko[b] and Lilin He[b]

[a]Universitá di Padova, Dipartimento di Fisica G. Galilei, Via Marzolo 8, I-35131 Padova, Italy, and [b]Neutron Scattering Sciences Division, Oak Ridge National Laboratory, Oak Ridge, Tennessee 37831-6393, USA. Correspondence e-mail: ciccariello@pd.infn.it

Analysis of the tails of the small-angle neutron scattering (SANS) intensities relevant to samples formed by porous silica and carbon dioxide at pressures ranging from 0 to 20 MPa and at temperatures of 308 and 353 K confirms that the CO_2 fluid must be treated as a two-phase system. The first of these phases is formed by the fluid closer to the silica wall than a suitable distance δ and the second by the fluid external to this shell. The sample scattering-length densities and shell thicknesses are determined by the Porod invariants and the oscillations observed in the Porod plots of the SANS intensities. The resulting matter densities of the shell regions (thickness 15–35 Å) are approximately equal, while those of the outer regions increase with pressure and become equal to the bulk CO_2 at the higher pressures only in the low-temperature case.

1. Introduction

Air rarefaction with increasing mount heights is well known to climbers. This likely is the simplest example of the general property that the density of a fluid is no longer homogeneous when the fluid molecules interact with an external field. For the same reason, the density profile of a fluid inside a vessel is not constant in proximity to the vessel walls. In fact, the walls of the container act as an external potential that ensures that no fluid molecule occupies a position external to the vessel. We defer to Percus (1982) for a statistical mechanical presentation of non-uniform fluids. Furthermore, the first numerical determinations of the density profile of a simple fluid near a hard wall trace back to the 1970s (see, *e.g.*, Abraham & Singh, 1977).

Wetting is another phenomenon intimately related to the behavior of a fluid near a solid wall. This issue was reviewed by de Gennes (1985), who stressed that the interaction of a wall with a fluid must be treated on a molecular basis since, at each point inside the vessel, it is equal to the statistical mechanical average of the interactions of the wall's and the fluid's molecules. The important role of the polarizability of the molecules was also underlined. Even though the discussion was carried out assuming that the vessel walls were plane and infinitely large, de Gennes (1985) emphasized that wetting of porous solids is far more interesting for its important practical implications, such as, for example, oil recovery from porous sands in oil fields. Unfortunately the theoretical treatment of the subject is still at a preliminary stage.

In any case, it is quite reasonable that the density profile of a fluid within a porous solid qualitatively behaves as shown in Fig. 1 along any direction orthogonal to the wall of the solid. This profile is largely inspired by those shown in Fig. 6 of the paper by Cai *et al.* (2008). These profiles were obtained by grand-canonical Monte Carlo (MC) simulations and refer to methane close to a graphitic plane wall. The presence of one or more oscillations close to the wall is a general finding. In the simplest cases of a fluid in contact with plane walls, these oscillations have been experimentally observed by measuring the force between two macroscopic solid plane walls separated by a very thin film of fluid (Israelashvili, 1982) or by X-ray experiments (Huisman *et al.*, 1997). [See also Nygård *et al.* (2009).]

These experiments cannot be carried out in the case of porous-solid/fluid systems because of the absence of macroscopic plane walls. Nonetheless it has recently been shown that useful structural information on these systems can be obtained by small-angle scattering experiments using X-rays (Jähnert *et al.*, 2009, and references therein) or neutrons (Smarsly *et al.*, 2001; Melnichenko *et al.*, 2006, 2009; Rother *et al.*, 2007; Melnichenko & Wignall, 2009; Radlinski *et al.*, 2009). In particular, after measuring the radiation absorption factors and the Porod invariants of some samples formed by porous silica with carbon dioxide at different pressures, Melnichenko *et al.* (2006) definitely showed, independently of the shape of the silica pores, that the variation of the aforesaid quantities with the CO_2 pressure requires that the fluid be treated as a two-phase system. Since the best spatial resolution of small-angle scattering (SAS) experiments is of the order of 10 Å (Guinier & Fournét, 1955), these experiments can only determine the scattering density profile averaged over spherical regions of diameters not smaller than 10 Å. [Note that by 'scattering density' we mean the scattering-length density or the electron density depending on whether we deal with neutron (SANS) or X-ray (SAXS) small-angle scattering.]

In this respect it is useful to recall a result proved by Ciccariello (2002) and related to the problem of approx-

imating a continuous function by a discrete valued function, *i.e.* a function that, in the simplest case, assumes two single values. This problem is of central importance for SAS experiments because, in interpreting the measured intensities, one usually assumes that the sample is made up of a few homogeneous phases (Debye *et al.*, 1957), where a few means two in most cases. Ciccariello's paper reported the equations that determine the best discrete valued approximation to a continuous scattering density function. The equations are based on the spatial averages of the last function and the unknown quantities are the sets over which the spatial averages are evaluated.

Consider now a sample formed by a porous silica and supercritical CO_2. The scattering density of this system takes a given value within the silica that, by assumption, is non-fractal so that its walls are sharply defined. Within the fluid and along each half-line orthogonal to the silica walls the density profile of the fluid will have a form similar to that shown in Fig. 1. Moreover, the surface of the porous silica can be considered plane if its curvature radii (and the silica pore diameters) are large enough to ensure that Porod's law is obeyed in the outer q range. These assumptions imply that (*a*) the SAS intensity of the porous silica obeys Porod's law in the scattering vector range $q > 0.065$ Å^{-1} if the pore diameters are larger than 50 Å (as happens in the cases that we shall consider later; see §4) and (*b*) the fluid profiles along any half-line orthogonal to the silica surface are expected to coincide. Item (*b*) ensures that a two-value approximation of the scattering density of the fluid, obtained by Ciccariello's procedure, will produce a first region of (suitable) thickness δ next to the silica wall with constant scattering density n_3 [equal to the mean value of the true scattering density $n(\mathbf{r})$ throughout the volume V_3 of this region, *i.e.* $n_3 = \int_{V_3} n(\mathbf{r})\,\mathrm{d}v/V_3$] and a remaining region V_2 of fluid with scattering density n_2, equal to the mean of the real fluid density over region V_2. The choice of the thickness value is made in such a way that the scattering intensity of the idealized system is closest (in the L_2 norm) to the observed one. By this idealization, the fluid region next to the silica is delimited by two parallel surfaces. Consequently, the second derivative of the correlation function of the resulting idealized system has a finite discontinuity at $r = \delta$ (Wu & Schmidt, 1974; Ciccariello, 1985). The analytical expression of the discontinuity, denoted here by $\mathcal{D}$, depends on the scattering densities of the three phases and on the area of the silica surface (Ciccariello, 1991). The noted discontinuity is also responsible for a further $O(q^{-4})$ term, besides the well known Porod one, in the asymptotic behavior of the scattering intensity at large q. In the Porod plot this extra term has the very simple oscillatory form $\mathcal{D}\cos(\delta q)$, so δ and $\mathcal{D}$, respectively, determine the 'frequency' and the amplitude of the extra oscillatory term. Since $\mathcal{D}$ depends on the phase scattering densities it appears evident that numerical analysis of the tails of the observed intensities can be used to determine the thickness and the scattering density values.

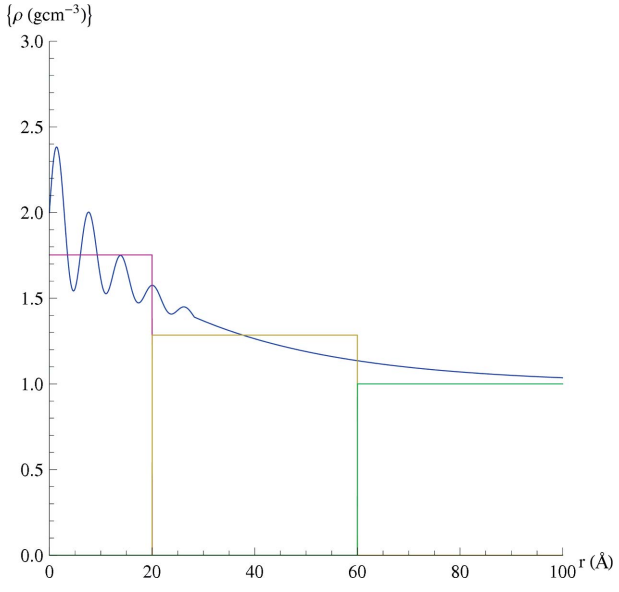

Figure 1
Schematic density profile of a fluid near a wall. The three horizontal segments represent the mean value of the profile in the corresponding intervals (note that the outermost one was considered infinitely large). They might correspond to a three-phase idealization of the density profile.

The aim of this paper is to show that this is in fact the case. For completeness it must be mentioned that the first application of this asymptotic analysis was performed by analyzing some glass intensities (Ciccariello & Benedetti, 1986). Subsequently it was used to characterize the films coating some porous silicas (Benedetti & Ciccariello, 1994; Pikus *et al.*, 2003). In this paper we shall fully exploit the potentialities of the procedure because, in contrast to the just mentioned cases, we shall analyze now intensities known in absolute units.

The plan of the paper is as follows. In the next section we describe in some detail the samples we are concerned with and the measurements performed on them. In §3 we report the main mathematical equations by giving also the expressions of the scattering densities in terms of the parameters determined by the best fits of the intensities. In §4, we combine the last equations with the values of the Porod invariants and we arrive at the unique determination of the scattering densities of the idealized system. The physical implications of these numerical results are also briefly discussed. §5 draws our final conclusions.

2. Experimental details

A silica aerogel with a volume fraction $\varphi_1 = 0.08$ of silica (porosity 92%), a surface area of 400 m^2 g^{-1} and a nominal density of 0.2 g cm^{-3} was obtained from Oscellus Technologies, Livermore, CA, USA. The aerogel surface is known to be covered with numerous methoxy groups (Si—O—CH_3) formed during supercritical drying of the precursor gel in supercritical methanol (Tajiri *et al.*, 1995). The aerogel was shaped into a cylinder (17 mm in diameter and 10 mm in length) that fits tightly into a SANS high-pressure cell that has been used extensively for previous neutron scattering experiments with CO_2-saturated silica aerogels and xerogels (Melnichenko *et al.*, 2004, 2006; Melnichenko & Wignall,

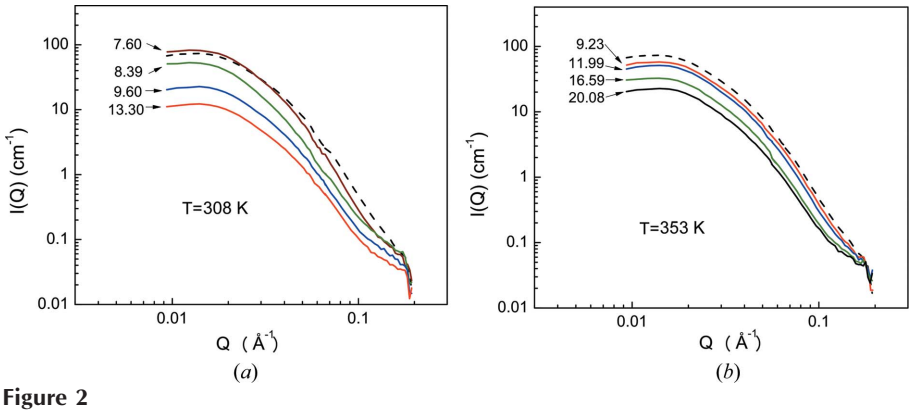

Figure 2
Representative SANS patterns for silica aerogel saturated with CO_2 as a function of pressure (MPa): (*a*) T = 308 K and (*b*) T = 353 K. Dashed lines represent scattering from pure aerogel.

2009). High-purity CO_2 (gas chromatography purity 99.99%) was obtained from Matheson Gas Products Inc. The pressure was measured using a precision digital pressure indicator (Sensotec, model AG-100) and the temperature of the cell was controlled to better than ±0.2 K.

SANS experiments were conducted at Oak Ridge National Laboratory (ORNL) on the General-Purpose SANS instrument (http://neutrons.ornl.gov/instruments/HFIR/CG2/) with a neutron wavelength λ of 4.8 Å ($\Delta\lambda/\lambda \simeq 0.13$). The sample–detector distance was chosen to cover the scattering vector (q) range $0.009 < q < 0.20$ Å^{-1}, where $q = (4\pi/\lambda)\sin(\theta/2)$, in which θ is the scattering angle. The data were corrected for instrumental background as well as detector efficiency and put on an absolute scale [cross section $I(q)$ in units of cm^{-1}] by means of pre-calibrated secondary standards (Wignall & Bates, 1987). Representative SANS data from the studied aerogels at two temperatures, T = 308 and 353 K, as a function of CO_2 pressure are shown in Fig. 2.

3. Model and related theoretical relations

Based on the considerations reported in §1 we shall idealize the sample as made up of three homogeneous phases, namely the silica, and the adsorbed and the confined bulk fluids. The adsorbed and the confined bulk fluids are, respectively, formed by the fluid molecules that are distant from the silica wall by less or more than δ, a distance to be determined by the best fit of the SAS intensities. We denote by 'confined bulk' fluid the fluid that lies within regions external to the shell but internal to the silica pores, because one expects that the mean interaction of the relevant fluid molecules with those of the walls is not yet fully negligible as happens in the bulk fluid case. Again the assumption that the pore size is around 50 Å implies, with reference to Fig. 1, that the adsorbed and the confined bulk fluids correspond to the first two regions there shown and that the bulk region (the outermost one in Fig. 1) is not present in our samples. As already anticipated, we also assume that the silica wall is a smooth surface and its curvature radii are larger than 50 Å so as to observe the asymptotic Porod behavior in the outer part of the explored q range (see §4). The first assumption implies that the sample presents two interfaces instead of three. In fact, denoting the silica phase by 1, the confined bulk fluid by 2 and the adsorbed fluid by 3, phase 1 is nowhere in contact with phase 2 so that the corresponding interface $S_{1,2}$ (where the index values refer to the opposing phases) does not exist. Thus, the only interphase surfaces are $S_{1,3}$ and $S_{2,3}$. Furthermore these surfaces are separated by a distance δ, constant along each straight line orthogonal to both surfaces. Hence, the two surfaces are parallel to each other and $\gamma''(r)$, the second derivative of the correlation function of the sample, will have a finite discontinuity at $r = \delta$. The expression of the discontinuity depends on the area S of the surface that is midway between $S_{1,3}$ and $S_{2,3}$ as well as on the scattering densities of the three phases (Ciccariello, 1991). The discontinuity is responsible for an oscillatory contribution, besides the well known Porod one, in the leading asymptotic behavior of the SAS intensity $I(q)$. In fact, the full expression of the leading asymptotic term [see equation (7) of Pikus *et al.* (2003)] is

$$I(q) = (\mathcal{A}/q^4)[1 + \mathcal{R}(\nu)\cos(q\delta)] + \mathcal{B}_{ck}, \tag{1}$$

with

$$\mathcal{A} \equiv 2\pi S n_{1,2}^2 \alpha(\nu)/V, \tag{2}$$

$$\mathcal{R}(\nu) \equiv (1-\nu^2)/(1+\nu^2), \quad \alpha(\nu) \equiv (1+\nu^2)/2, \tag{3}$$

$$\nu \equiv (n_{1,3} - n_{3,2})/n_{1,2} \quad \text{and} \quad n_{i,j} \equiv n_i - n_j, \ i,j = 1,2,3. \tag{4}$$

Here, V denotes the sample volume, n_i the scattering density (*i.e.* the electron density for SAXS experiments or the scattering-length density for SANS experiments) of the ith phase and $\mathcal{B}_{ck}$ the background contribution due to the microscopic density fluctuations (Luzzati *et al.*, 1961). In obtaining equation (1) it is assumed that δ is much smaller than the curvature radii so as to have

$$S \simeq S_{1,3} \simeq S_{2,3} \quad \text{and} \quad V_3 \simeq \delta S, \tag{5}$$

where V_3 denotes the volume of phase 3 (the adsorbed fluid film).

Parameters $\mathcal{A}$, $\mathcal{R}$, δ and $\mathcal{B}_{ck}$ can be determined by best-fitting the observed scattering intensity to equation (1) within the outer scattering vector interval $[q_m, q_M]$, to be suitably chosen [see the discussion below equation (24)]. The expression of the Porod invariant for a three-phase sample in terms of the volume fractions $\varphi_i = V_i/V$ and scattering densities n_i is

$$\mathcal{Q}_{Prd} \equiv \int_0^\infty q^2 I(q)\,dq = 2\pi^2(n_{1,2}^2\varphi_1\varphi_2 + n_{1,3}^2\varphi_1\varphi_3 + n_{2,3}^2\varphi_2\varphi_3). \tag{6}$$

This is numerically evaluated by the observed intensity values I_j, relevant to the scattering vector values q_j, by the expression

$$\mathcal{Q}_{\rm Prd} = \left[\sum_{q_j \le q_{\rm M}} q_j^2 (I_j - \mathcal{B}_{\rm ck})(q_j - q_{j-1}) \right] + \mathcal{A}/q_{\rm M} \qquad (7)$$

(where we put $q_0 = 0$ and we neglect the contribution related to $\mathcal{R}$ since it is much smaller than that related to $\mathcal{A}$).

In our case the scattering density of the porous silica is known. Thus, it is convenient to introduce the dimensionless scattering densities $\hat{n}_j$ and the sample specific surface $\mathcal{S}$ according to the definitions

$$\hat{n}_2 \equiv n_2/n_1, \quad \hat{n}_3 \equiv n_3/n_1 \quad \text{and} \quad \mathcal{S} \equiv S/V. \qquad (8)$$

The quantity ν becomes

$$\nu = (1 + \hat{n}_2 - 2\hat{n}_3)/(1 - \hat{n}_2), \qquad (9)$$

while expression (7), using the condition $\varphi_1 + \varphi_2 + \varphi_3 = 1$ and equation (5), becomes

$$\mathcal{Q}_{\rm Prd} = 2\pi^2 n_1^2 [(1 - \hat{n}_2)^2 \varphi_1 (1 - \varphi_1 - \varphi_3) + (1 - \hat{n}_3)^2 \varphi_1 \varphi_3 + (\hat{n}_2 - \hat{n}_3)^2 (1 - \varphi_1 - \varphi_3)\varphi_3]. \qquad (10)$$

By equations (9), (2) and (3) one finds the following expressions of $\mathcal{A}$ and $\mathcal{R}$ in terms of $\hat{n}_2$ and $\hat{n}_3$:

$$\mathcal{A} = 2\pi n_1^2 \mathcal{S}(1 - 2\hat{n}_3 - 2\hat{n}_2\hat{n}_3 + \hat{n}_2^2 + 2\hat{n}_3^2), \qquad (11)$$

$$\mathcal{R} = \frac{2(\hat{n}_2 - \hat{n}_3)(\hat{n}_3 - 1)}{1 - 2\hat{n}_3 - 2\hat{n}_2\hat{n}_3 + \hat{n}_2^2 + 2\hat{n}_3^2}. \qquad (12)$$

These can be solved in order to express $\hat{n}_2$ and $\hat{n}_3$ in terms of $\mathcal{A}$ and $\mathcal{R}$, besides $\mathcal{S}$ and n_1. One finds four solutions that read

$$\hat{n}_{2,\rm I} = 1 + \mathcal{D}_-(\mathcal{R} + \Delta_+), \quad \hat{n}_{3,\rm I} = 1 + \mathcal{D}_-, \qquad (13)$$

$$\hat{n}_{2,\rm II} = 1 - \mathcal{D}_-(\mathcal{R} + \Delta_+), \quad \hat{n}_{3,\rm II} = 1 - \mathcal{D}_-, \qquad (14)$$

$$\hat{n}_{2,\rm III} = 1 + \mathcal{D}_+(\mathcal{R} + \Delta_-), \quad \hat{n}_{3,\rm III} = 1 + \mathcal{D}_+, \qquad (15)$$

$$\hat{n}_{2,\rm IV} = 1 - \mathcal{D}_+(\mathcal{R} + \Delta_-), \quad \hat{n}_{3,\rm IV} = 1 - \mathcal{D}_+, \qquad (16)$$

where we put

$$\Delta_\pm \equiv 1 \pm (1 - \mathcal{R}^2)^{1/2} \qquad (17)$$

and

$$\mathcal{D}_\pm \equiv \frac{1}{2n_1\mathcal{R}} \left(\frac{\mathcal{A}\Delta_\pm}{\pi\mathcal{S}} \right)^{1/2}. \qquad (18)$$

For each of the above solutions, its substitution into the right-hand side (r.h.s.) of equation (10) gives an expression whose unknown quantities are only φ_1 and $\mathcal{S}$, because n_1 is assumed to be known and δ was determined by the fit of the observed intensity to the r.h.s. of equation (1). More explicitly, after putting

$$\mathcal{E}(\mathcal{S}, \varphi_1, \varphi_3; \mathcal{A}, \mathcal{R}) \equiv \frac{\pi\mathcal{A}\{(1 - \varphi_3)[\varphi_3 + 2(1 + \mathcal{R})\varphi_1] - 2\varphi_1^2(1 + \mathcal{R})\}}{2\mathcal{S}} \qquad (19)$$

and

Table 1
Temperature, pressure and density data for the measured samples.

No.: index of the analyzed samples; T: temperature in K; P: CO_2 pressure in MPa; ρ_0: density of the CO_2 at the reported pressure; ρ_2: density of the 'bulk' CO_2 within the pores of the silica; ρ_3: density of the CO_2 film adsorbed on the silica walls; φ_2: volume fraction of the confined bulk fluid; and φ_3: volume fraction of the adsorbed fluid. The values reported in columns 2, 3 and 4 were experimentally observed. Those in columns 4, 5, 6 and 7 follow from the analysis of the observed SANS intensities by the procedure described in the paper and their units are g cm^{-3}.

No.	T	P	ρ_0	ρ_2	ρ_3	φ_2	φ_3
1	308	0.00	0.000	0.000 (1)	0.000 (1)	–	–
2	308	4.61	0.105	0.288 (71)	0.922 (54)	0.62	0.30
3	308	6.63	0.193	0.390 (64)	1.039 (34)	0.57	0.36
4	308	7.60	0.291	0.434 (49)	1.149 (17)	0.37	0.55
5	308	7.92	0.387	0.465 (41)	1.146 (12)	0.29	0.63
6	308	8.01	0.437	0.537 (37)	1.175 (11)	0.28	0.64
7	308	8.11	0.491	0.568 (39)	1.183 (12)	0.25	0.67
8	308	8.39	0.591	0.718 (43)	1.241 (15)	0.30	0.62
9	308	9.60	0.697	0.729 (39)	1.197 (15)	0.21	0.72
10	308	13.30	0.793	0.748 (41)	1.241 (15)	0.29	0.64
11	353	0.00	0.000	0.420 (23)	1.202 (43)	–	–
12	353	5.38	0.096	0.313 (52)	1.142 (15)	0.51	0.42
13	353	9.23	0.196	0.366 (62)	1.153 (22)	0.42	0.50
14	353	11.99	0.296	0.458 (46)	1.170 (14)	0.36	0.57
15	353	14.15	0.390	0.510 (40)	1.165 (12)	0.31	0.62
16	353	15.63	0.454	0.619 (43)	1.189 (15)	0.39	0.53
17	353	16.59	0.493	0.721 (55)	1.215 (23)	0.47	0.45
18	353	20.08	0.597	0.775 (74)	1.092 (86)	0.65	0.27

$$\mathcal{F}(\mathcal{S}, \varphi_1, \varphi_3; \mathcal{A}, \mathcal{R}) \equiv \frac{\pi\mathcal{A}\varphi_3[(1 - \varphi_3 - 2\varphi_1)(1 - \mathcal{R}^2)^{1/2}]}{2\mathcal{S}}, \qquad (20)$$

from equation (10) it results that

$$\mathcal{Q}_{\rm Prd} = \mathcal{E}(\mathcal{S}, \varphi_1, \varphi_3; \mathcal{A}, \mathcal{R}) + \mathcal{F}(\mathcal{S}, \varphi_1, \varphi_3; \mathcal{A}, \mathcal{R}) \qquad (21)$$

or

$$\mathcal{Q}_{\rm Prd} = \mathcal{E}(\mathcal{S}, \varphi_1, \varphi_3; \mathcal{A}, \mathcal{R}) - \mathcal{F}(\mathcal{S}, \varphi_1, \varphi_3; \mathcal{A}, \mathcal{R}), \qquad (22)$$

depending on whether one of the first two roots [*i.e.* equation (13) or (14)] or one of the second two [*i.e.* equation (15) or (16)] is substituted in the r.h.s. of equation (10). Since $\mathcal{Q}_{\rm Prd}$ is numerically determined by equation (7), for any sample each of the two final expressions of equation (10) yields an equation that can be used to determine $\mathcal{S}$ if φ_1 is known. In fact, φ_3 and φ_2 are simply related to $\mathcal{S}$ because from equations (5) and (9) it immediately follows that

$$\varphi_3 = \mathcal{S}\delta \quad \text{and} \quad \varphi_2 = 1 - \varphi_1 - \mathcal{S}\delta. \qquad (23)$$

If φ_1 is not known (or we do not want to use this value in order to test the accuracy of the best-fit analysis) we can determine both $\mathcal{S}$ and φ_1 if we know at least two SAS intensities that refer to samples that only differ among themselves for the scattering densities of phases 2 and 3. This is exactly what happens in the case of the samples obtained using a cell containing a given amount of porous silica which is then filled up with carbon dioxide at different pressure values. It should now appear clear why the use of equation (1) allows us to determine the (average) scattering densities of the adsorbed and the confined bulk carbon dioxide within the porous silica

at different pressures. The details of the numerical analysis are illustrated in the following section. We stress that our analysis assumes that the geometrical configuration and the scattering density of the silica phase do not appreciably change when filled with carbon dioxide at different pressures. In fact, the comparison of the SAS intensities before and after CO_2 exposure proves that the silica aerogel structure remains unaffected by supercritical CO_2 (Melnichenko *et al.*, 2006). In the presence of the fluid, the silica undergoes a uniform compression that, owing to the small compressibility, will yield a reasonably small uniform volume contraction and a small increase of the scattering density. We shall consider these effects negligible.

4. Numerical analysis

As already mentioned, we shall analyze a set of SANS spectra that refer to a cell containing a porous silica powder when the cell is filled by CO_2 at different pressures and temperatures. The values of the temperature (in K), the pressure (in MPa) and the density (in g cm^{-3}) are reported in the second, third and fourth columns of Table 1, respectively. The integer in the first column numbers the samples.

The Porod plots of the intensities are shown in Fig. 3 for the samples at T = 308 K and in Fig. 4 for those at 353 K. In both figures the thin curves plot the asymptotic expression given by equation (1) with the values of the involved parameters $\mathcal{A}$, $\mathcal{R}$, δ and $\mathcal{B}_{ck}$ such as to make the value of the expression

$$\chi^2_{intst} = \sum_{q_m \le q_j \le q_M} \{q_j^4 I_j - \mathcal{A}[1 + \mathcal{R}\cos(q_j\delta)] - q_j^4 \mathcal{B}_{ck}\}^2 \qquad (24)$$

as small as possible. Here I_j are the intensity values relevant to one of the listed samples, and q_m and q_M, respectively, denote the lowest and highest bounds of the best-fitted q range. For each intensity these values are made visible by the fact that the thin curves have only been drawn within the best-fitted q range. We took $q_M = 0.18$ Å^{-1} because beyond this value the parasitic scattering from the high-pressure cell edges obscures the SANS intensities. The smallest bound q_m was put at approximately the peak position.

The best-fitted parameter values are reported in Table 2, together with the χ^2_{intst} values (see the caption). Definition (24)

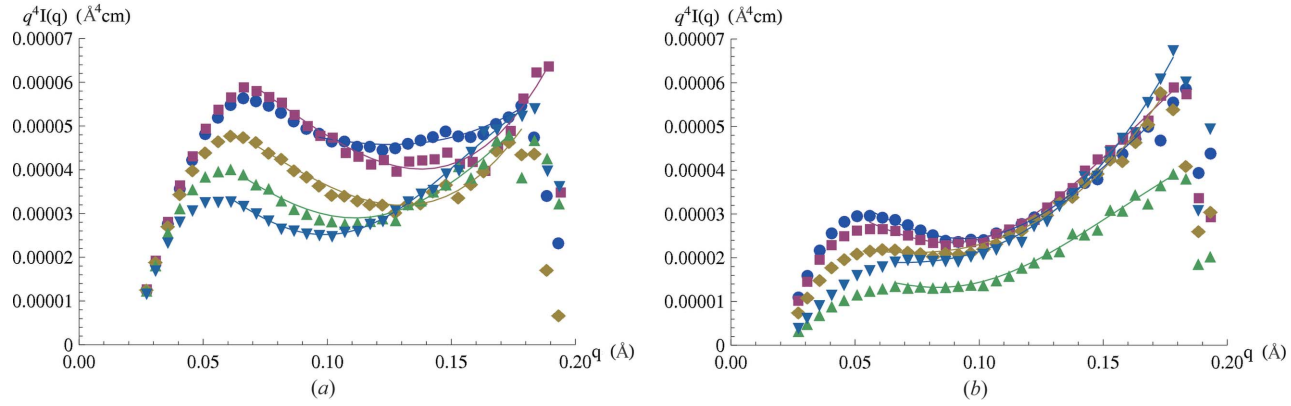

Figure 3
Porod plots of the scattering intensities relevant to the samples at T = 308 K filled up with CO_2 at different pressures P. (*a*) Circles: P = 0 Pa; squares: 4.61 MPa; diamonds: 6.63 MPa; triangles-up: 7.60 MPa; triangles-down: 7.92 MPa. (*b*) Circles: 8.01 MPa; squares: 8.11 MPa; diamonds: 8.39 MPa; triangles-up: 9.60 MPa; triangles-down: 13.30 MPa. The continuous curves represent the theoretical results obtained by best fitting the observed intensities to the asymptotic expression given by equation (1). They have only been drawn within the q ranges used for the best fits.

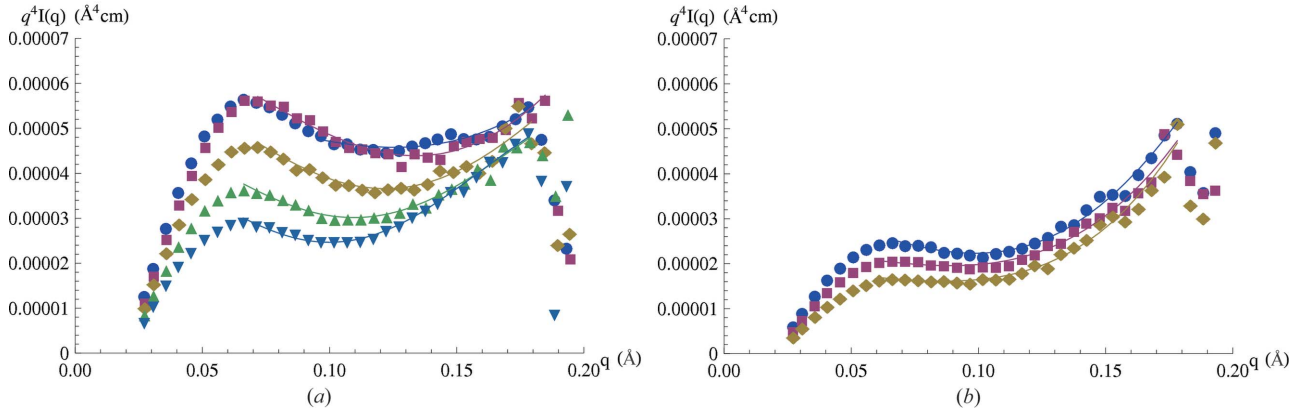

Figure 4
Porod plots of the scattering intensities relevant to the samples at T = 353 K filled up with CO_2 at different pressures P. (*a*) Circles: P = 0 Pa; squares: 5.38 MPa; diamonds: 9.23 MPa; triangles-up: 11.98 MPa; triangles-down: 14.15 MPa. (*b*) Circles: 15.63 MPa; squares: 16.59 MPa; diamonds: 20.08 MPa. The continuous curves represent the best-fit results.

Table 2
Results of the intensity best fits by equation (24).

The units for $\mathcal{A}$, δ and $\mathcal{B}_{ck}$ are Å^{-4} cm^{-1}, Å and cm^{-1}, respectively.

No.	$\chi^2_{intst} \times 10^{13}$	$\mathcal{A} \times 10^5$	$\mathcal{R}$	δ	$\mathcal{B}_{ck}$
1	9.82	4.84	0.171	19.0	0.0135
2	44.3	4.11	0.842	15.0	0.0435
3	34.3	3.72	0.632	17.6	0.0352
4	16.2	4.13	0.327	27.3	0.0071
5	6.16	3.77	0.349	31.2	0.0059
6	3.80	3.26	0.292	31.8	0.0148
7	7.53	3.04	0.273	33.4	0.0198
8	13.6	2.16	0.106	30.9	0.0370
9	9.15	1.77	0.299	35.4	0.0158
10	12.3	1.92	0.115	31.6	0.0445
11	9.82	4.84	0.171	19.0	0.0135
12	19.2	5.54	0.301	20.8	0.0127
13	48.5	4.98	0.288	24.9	0.0048
14	12.5	4.07	0.274	28.0	0.0039
15	5.84	3.47	0.308	30.7	0.0059
16	10.8	2.61	0.276	26.4	0.0252
17	28.9	1.94	0.217	22.5	0.0303
18	28.5	1.04	0.854	13.6	0.0428

is not the statistically correct one because we do not know the experimental errors on I_j. This explains the very small values found for χ^2_{intst}. However, Figs. 3 and 4, and the fact that the values given in the second column of Table 2 are of the same order, make us confident of the good quality of the fits.

The parameter values are shown in Fig. 5. The corresponding errors are shown by the error bars. They are smaller than the symbol size when the bars are not visible (a convention adopted throughout the paper). They have been estimated from the Hessian values evaluated at the relevant minima of χ^2_{intst} (scaled to one). The behavior of the parameters changes with temperature and with the CO_2 pressure. At 353 K the thickness of the adsorbed CO_2 shows a well defined maximum, while the maximum is much broader at 308 K. Moreover, the peak position increases with temperature, while its height slightly decreases. We note that a finite thickness is also present at zero pressure. This is probably due to the presence of water and methoxy groups adsorbed on the silica walls. The behaviors of $\mathcal{A}$ at low and high temperatures are roughly similar, even though the behavior appears more regular at 353 K. The value of $\mathcal{R}$ is almost constant at 353 K and much more variable at 308 K. The behavior of $\mathcal{B}_{ck}$ is much more irregular, aside from a tendency to show a minimum and then an increase with pressure.

Fig. 6 shows the values of $\mathcal{Q}_{Prd}$, the Porod invariant relevant to each considered sample. The $\mathcal{Q}_{Prd}$ values have been evaluated by equation (9). From the behaviors of all these parameters it is difficult to draw definite physical consequences because these quantities depend on many variables. However, one feature appears evident from Figs. 5 and 6: the involved quantities show a strong dependence on the pressure within the range 8–9 Mpa at 308 K only. (The same feature is also evident in the left panel of Fig. 7.) Under these physical conditions the bulk CO_2 is still close to its critical point. This suggests that the noted strong dependence is likely related to the higher compressibility and larger density fluctuations shown by the fluid around the critical region.

It is now important to use the values of $\mathcal{A}$, $\mathcal{R}$ and δ to determine the (matter) density values of the CO_2 phases present within the samples. We already noted that the relative scattering-length densities of phases 2 and 3 are given by equations (13)–(16). These involve, however, quantities $\mathcal{D}_+$ or $\mathcal{D}_-$ which depend on $\mathcal{S}$ and n_1, respectively, the specific surface and the scattering-length density of the porous silica [see

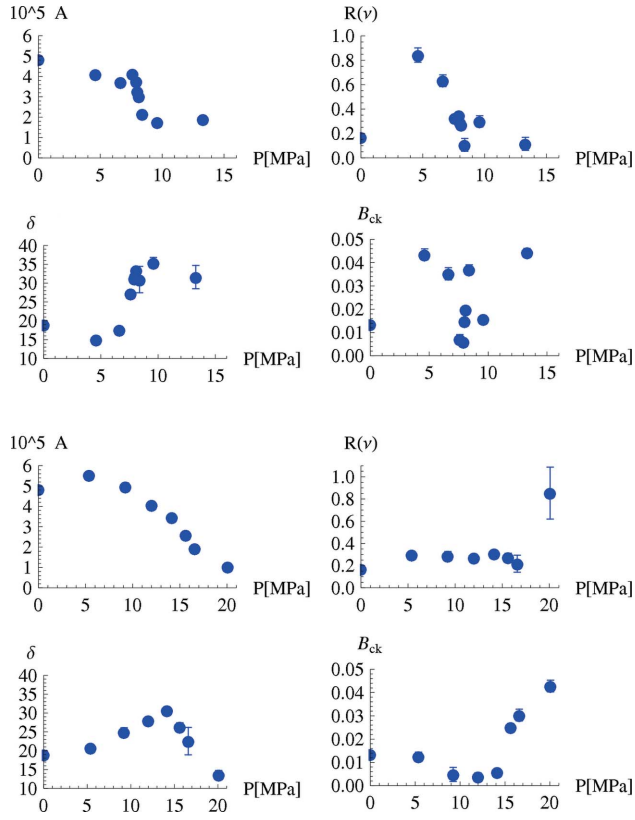

Figure 5
Plots of the best-fitted parameter values reported in Table 2 *versus* the CO_2 pressure. The four figures at the top refer to the sample at T = 308 K and the four at the bottom to the samples at T = 353 K. The errors are smaller than the symbol size when the error bars are not visible. The units of $\mathcal{A}$, δ and $\mathcal{B}_{ck}$, respectively, are Å^{-4} cm^{-1}, Å and cm^{-1}.

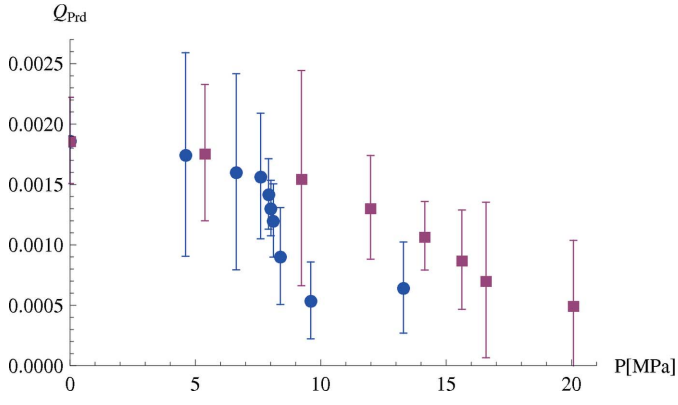

Figure 6
Plot of the sample Porod invariants, evaluated by equation (9), *versus* the CO_2 pressure. Filled dots refer to the samples at T = 308 K, filled squares to those at T = 353 K. The $\mathcal{Q}_{Prd}$ units are Å^{-3} cm^{-1}.

equation (18)]. While n_1 is known to be equal to 3.16×10^{10} cm^{-2}, because the scattering length and the matter density of the porous silica are, respectively, equal to 1.58×10^{-12} cm and 2 g cm^{-3}, as yet quantity $\mathcal{S}$ is not known. Thus, the relative scattering-length densities of phase 2 and 3 are only known in terms of $\mathcal{S}$. This quantity, as well as the volume fraction of the silica, can be obtained from the known $\mathcal{Q}_{\rm Prd}$ values. This fact in turn will allow us to determine the scattering-length and the matter densities of the adsorbed and confined bulk-fluid phases of the samples.

In fact, denoting by $\mathcal{Q}_{{\rm Prd},J}$ the Porod invariant of sample J with $J = 1, \ldots, 18$, the values of $\mathcal{S}$ and φ_1 are obtained by minimizing both the function

$$\chi^2_{\rm fnl,+} \equiv \frac{1}{14} {\sum_{J=2,18}}' \left\{ \mathcal{Q}_{{\rm Prd},J} - [\mathcal{E}(\cdot; \mathcal{A}_J, \mathcal{R}_J) + \mathcal{F}(\cdot; \mathcal{A}_J, \mathcal{R}_j)] \right\}^2 \tag{25}$$

and the function

$$\chi^2_{\rm fnl,-} \equiv \frac{1}{14} {\sum_{J=2,18}}' \left\{ \mathcal{Q}_{{\rm Prd},J} - [\mathcal{E}(\cdot; \mathcal{A}_J, \mathcal{R}_J) - \mathcal{F}(\cdot; \mathcal{A}_J, \mathcal{R}_j)] \right\}^2, \tag{26}$$

where the prime on the sum symbol denotes that the value $J = 11$ has not been considered and $\cdot$ stands for the quantities $(\mathcal{S}, \varphi_1, \varphi_3) = (\mathcal{S}, \varphi_1, \mathcal{S}\delta)$. Samples 1 and 11 are porous silica with no carbon dioxide. After minimizing function (25), one finds

$$\begin{aligned} &\chi^2_{\rm fnl,+} = 2.64 \times 10^{-5}, \quad \mathcal{S} = 2.02\,(15) \times 10^6\ {\rm cm}^{-1} \\ &\text{and} \quad \varphi_1 = 0.0748\,(768). \end{aligned} \tag{27}$$

If one performs the minimization by also including samples 1 and 11 in definition (25), one finds $\chi^2_{\rm fnl,+} = 2.48 \times 10^{-5}$, $\mathcal{S} = 2.02\,(14) \times 10^6$ cm^{-1} and $\varphi_1 = 0.072\,(73)$. These values are close to the previous ones. It appears reasonable to conclude that whatever the choice of $\chi^2_{\rm fnl,+}$ the final results do not appreciably change. Since we do not know much about the chemical impurities present inside the porous silica after its chemical preparation we prefer to refer to definitions (25) and (26) because these only involve the samples containing CO_2. The minimization of expression (26) gives

$$\begin{aligned} &\chi^2_{\rm fnl,-} = 1.37 \times 10^{-5}, \quad \mathcal{S} = 2.16\,(10) \times 10^6\ {\rm cm}^{-1} \\ &\text{and} \quad \varphi_1 = 0.41\,(4). \end{aligned} \tag{28}$$

This solution is physically unsatisfactory because the resulting values of the volume fraction φ_3 $(= \mathcal{S}\delta)$ are such that, added to the value of φ_1, they exceed one. Moreover, the φ_1 value of 0.41 does not agree with that obtained by weight and volume measurements (0.08, as reported in §2). Hence the physically acceptable solution is that given by relations (27).

The relative scattering-length densities of phases 2 and 3 are obtained by equations (13) or (14), substituting here the known n_1 value, the just obtained $\mathcal{S}$ value, and the $\mathcal{A}$ and $\mathcal{R}$ values previously determined. Finally, the matter density values of phases 2 and 3 are obtained, in units of g cm^{-3}, by multiplying the resulting scattering-length density values by $n_1 M_{CO_2}/(\mathcal{N}_A b_{CO_2}) = 1.272$, where M_{CO_2} denotes the molecular weight of the carbon dioxide, b_{CO_2} $(= 1.81 \times 10^{-12}{\rm cm}^{-1})$ its scattering length and $\mathcal{N}_A$ the Avogadro number. It turns out that the matter densities resulting from equation (13) for the adsorbed and the confined bulk fluids physically are not satisfactory for two reasons: (*a*) for both phases they are greater than that of the bulk CO_2 (and even of the silica), and (*b*) they decrease as the pressure increases. Thus only the densities resulting from equation (14) are the physically correct solutions. The corresponding values are reported with their errors in Table 1 and are shown in Fig. 7. [The errors have been estimated as described in the case of Table 2.] The figure makes it evident that (*a*) the matter density of the adsorbate is relatively insensitive to the CO_2 pressure since whatever the latter value it is roughly equal to 1.2 g cm^{-3}, and (*b*) the matter density of phase 2, *i.e.* the confined bulk CO_2, increases with pressure. Furthermore, at T = 308 K (see the left panel of Fig. 7), the matter density approaches the bulk CO_2 values from above as the pressure increases and practically coincides with the bulk values at 9.6 and 13.3 MPa. At T = 353 K (right panel of Fig. 7), the confined bulk CO_2 density is greater than the bulk's but, in contrast to the previous case, the difference is almost constant throughout the explored pressure range.

This behavior is worth a few words of comment. In the introductory section we emphasized that, if a fluid wets a solid wall, the latter molecules tend to attract the fluid's more

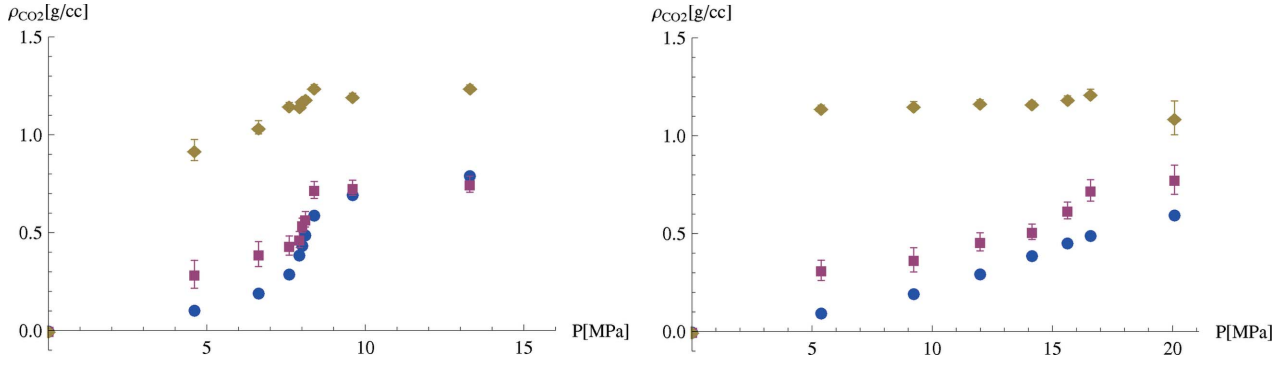

Figure 7
Plots of the matter density values of the CO_2 phases *versus* the CO_2 pressure. Filled circles: bulk CO_2 phase within a large vessel; filled squares: bulk confined CO_2; diamonds: density of the CO_2 film adsorbed on the silica wall. Left: samples at T = 308 K; right: samples at T = 353 K.

strongly than the fluid molecules do among themselves. We recall that the attraction originates from the molecule polarizabilities and, as happens for the Lennard–Jones potential, this attraction represents the tail of the molecule–molecule effective interaction (see, *e.g.*, Hansen & McDonald, 1976). We also recall that (i) given a (bulk) fluid at fixed temperature and pressure, if the interaction between the particles becomes more attractive (repulsive) the density increases (decreases); (ii) at fixed density and interactions an increase of the temperature causes an increase of the pressure and *vice versa*; and (iii) close to an ideally rigid wall (*i.e.* when the interaction between the molecules of the wall and those of the fluid is a hard-core one) the density profile is similar to that shown in Fig. 1 with the difference that the maximum is located at $r = 0$ [*i.e.* on the wall; see, *e.g.*, Abraham & Singh (1977) and Percus & Williams (1983)]. Because a higher density causes (and is produced by) a higher pressure, the last property implies that the pressure attains its maximum on the wall and decreases (with some oscillations) as one drifts away from the wall. The presence of such a maximum makes the approach to the wall very hard for the fluid molecules inside the vessel so that these remain confined within the vessel. In close proximity to the wall the last picture does not change in the presence of an attractive tail in the interaction of the real wall with the fluid because the repulsive forces are much stronger than the attractive ones. Recalling that n_3 and, consequently, ρ_3 result from an average of the true density profile in the vicinity of the wall, then to have found that the matter density of the adsorbed fluid is higher than that of the bulk and rather insensitive to the applied pressure appears quite sound. Furthermore, the mechanical statistical effects of the repulsive forces depend weakly on the temperature. (In fact, in the case of the ideal hard-sphere fluid, the temperature dependence only occurs by the kinetic contribution.) Thus, the fact that the found ρ_3 values are almost equal to 1 g cm^{-3}, whatever the temperature value, also is physically quite sensible.

The quantities n_2 and ρ_2 result from the average of the true profiles over intervals that go from δ to the mid-point of the pores. The latter diameters being $\sim$70 Å (Tajiri *et al.*, 1995), the distance range from the walls is [δ, 35 Å]. Here the attractive part of the wall–liquid interaction is still very effective. Thus, according to (i) above, one expects – as in fact happens – that the ρ_2 values will be greater than those of the bulk. Moreover, the difference between the two should decrease with increasing bulk pressure because an increase of the pressure leads to an increase of the density and, consequently, the role of the repulsive part of the interaction becomes more pronounced. This effect is clearly visible only at 308 K. Fig. 7 shows that the largest density of the bulk fluid at 353 K is considerably smaller than that at the lowest temperature. This implies that the attractive effects still dominate the repulsive ones at 353 K so as to make the confined bulk fluid density greater than that of the bulk throughout the explored pressure range, as is actually observed. In other words, this range must be further enlarged to observe the approach between the two densities.

5. Conclusion

SAS experiments have already indicated that a fluid inside a porous silica sample must be approximated by a two-phase system formed by a layer of constant density and thickness next to the wall of the solid support and a remaining region with a different density value. This conclusion was reached by exploiting the cylindrical shape of the pores (Smarsly *et al.*, 2001; Jähnert *et al.*, 2009) and independently from such assumptions (Melnichenko *et al.*, 2006). In the present paper, analyzing the tails of the observed intensities, we have gone a step farther, since we have been able to determine the thickness values and the density values of the fluid region closer to the silica wall as well as the density of the bulk fluid confined in the outer regions. The behavior of the values with temperature and pressure physically appears to be quite sound. These values represent the averages of the real density profiles of the fluid inside two complementary regions of the silica pores. Their determination is the main original aspect of this analysis.

Research at Oak Ridge National Laboratory's High Flux Isotope Reactor was sponsored by the Laboratory Directed Research and Development Program and the Scientific User Facilities Division, Office of Basic Energy Sciences, US Department of Energy. This research was supported in part by an appointment to the ORNL Postdoctoral Research Associates Program, administered jointly by the ORNL and the Oak Ridge Institute for Science and Education.

References

Abraham, F. F. & Singh, Y. (1977). *J. Chem. Phys.* **67**, 2384–2393.
Benedetti, A. & Ciccariello, S. (1994). *J. Appl. Cryst.* **27**, 249–256.
Cai, Q., Buts, A., Seaton, N. A. & Biggs, M. J. (2008). *Chem. Eng. Sci.* **63**, 3319–3327.
Ciccariello, S. (1985). *Acta Cryst.* A**41**, 560–568.
Ciccariello, S. (1991). *Phys. Rev. A*, **44**, 2975–2983.
Ciccariello, S. (2002). *Acta Cryst.* A**58**, 460–463.
Ciccariello, S. & Benedetti, A. (1986). *J. Appl. Cryst.* **19**, 195–197.
Debye, P., Anderson, H. R. & Brumberger, H. (1957). *J. Appl. Phys.* **20**, 518–523.
Gennes, P. G. de (1985). *Rev. Mod. Phys.* **57**, 827–863.
Guinier, A. & Fournét, G. (1955). *Small-Angle Scattering of X-rays.* New York: John Wiley.
Hansen, J. P. & McDonald, I. R. (1976). *Theory of Simple Liquids.* London: Academic Press.
Huisman, W. J., Peters, J. F., Zwanenburg, M. J., de Vries, S. A., Derry, E. D., Abernathy, D. & van der Veen, J. F. (1997). *Nature* (*London*), **390**, 379–381.
Israelashvili, J. N. (1982). *Adv. Colloid Interface Sci.* **16**, 31–47.
Jähnert, S., Müter, D., Prass, J., Zickler, G. A., Paris, O. & Findenegg, G. H. (2009). *J. Phys. Chem. C*, **113**, 15201–15210.
Luzzati, V., Witz, J. & Nicolajeff, A. (1961). *J. Mol. Biol.*, **3**, 367–371.
Melnichenko, Y. B., Mayama, H., Cheng, G. & Blach, T. (2009). *Langmuir*, **26**, 6374−6379.
Melnichenko, Y. B. & Wignall, G. D. (2009). *Int. J. Thermophys.* **30**, 1578–1590.
Melnichenko, Y. B., Wignall, G. D., Cole, D. R. & Frielinghaus, H. (2004). *Phys. Rev. E*, **69**, 057102.
Melnichenko, Y. B., Wignall, G. D., Cole, D. R. & Frielinghaus, H. (2006). *J. Chem. Phys.* **124**, 204711.
Nygård, K., Satapathy, D. K., Bunk, O., Perret, E., Buitenhuis, J., David, C. & van der Veen, J. F. (2009). *J. Appl. Cryst.* **42**, 1129–1138.

Percus, J. K. (1982). *The Liquid State of Matter*, edited by E. W. Montroll & J. L. Lebowitz. New York: North Holland.
Percus, J. K. & Williams, G. O. (1983). *J. Chem. Phys.* **79**, 3009–3017.
Pikus, S., Kobylas, E. & Ciccariello, S. (2003). *J. Appl. Cryst.* **36**, 744–748.
Radlinski, A. P., Bushbridge, T. L., Gray, E. M., Blach, T. P., Cheng, G., Melnichenko, Y. B., Cookson, D. J., Mastarlez, M. & Esterle, J. (2009). *Langmuir*, **25**, 2385–2389.
Rother, G., Melnichenko, Y. B., Cole, D. R., Frielinghaus, H. & Wignall, G. D. (2007). *J. Phys. Chem.* **111**, 15736–15742.
Smarsly, B. M., Goltner, C., Antonietti, M., Ruland, W. & Hoinkis, E. (2001). *J. Phys. Chem. B*, **105**, 831–840.
Tajiri, K., Igarashi, K. & Nishio, T. (1995). *J. Non-Cryst. Solids*, **186**, 83–87.
Wignall, G. D. & Bates, F. S. (1987). *J. Appl. Cryst.* **20**, 28–40.
Wu, H. & Schmidt, P. W. (1974). *J. Appl. Cryst.* **7**, 131–146.